






Integrating Safety With Performance in Connected Automated Truck Control: Experimental Validation

Anil Alan , Graduate Student Member, IEEE, Chaozhe R. He , Tamas G. Molnar , Member, IEEE, Joahan Chacko Mathew , A. Harvey Bell, and Gábor Orosz , Senior Member, IEEE

Abstract—Combining efficiency with safety is one of the most important design challenges for connected automated trucks. In order to address this challenge for longitudinal control problems, we propose a scheme that integrates a performance-based controller with a safety-oriented controller in a seamless manner. This safe integration scheme operates instantaneously, and it is compatible with a large class of controllers. We first link this practical integration method to the theoretical framework of control barrier functions that endows controllers with formal safety guarantees. Then, through this scheme we safely integrate a predictive-type controller minimizing energy consumption (predictive cruise control—PCC) with a safety-oriented cruise controller structure relying on connectivity (connected cruise control—CCC). Importantly, the efficacy of the safe and seamless integration between the PCC and the CCC is demonstrated using on-road experiments with a full-scale connected automated truck. Initial experimental campaign is held on a closed test track, and safe driving is achieved thanks to the CCC while up to 18% energy saving is obtained thanks to the PCC. Finally, experiments are extended to a public highway, and similar results are obtained with up to 4.3% energy saving.

Index Terms—Connected automated trucks, control barrier functions, energy efficiency, safety.

I. INTRODUCTION

THE rapid progress in automated vehicle (AV) technology is projected to lead to considerable amount of AVs on public roads in the foreseeable future, even with conservative estimates [1]. AVs are expected to bring prospects to individuals and society, including improved mobility, comfort, energy and

time efficiency, and a reduction in carbon emission [2], [3]. While each of these prospects pose essential objectives to be optimized in AV design, safety is yet to remain as the most critical requirement. Indeed, studies show that 93% of the total traffic accidents per year in the US are caused by human-related errors [4], which is a factor that can potentially be reduced or diminished with reliable AV technologies [5].

Safety in commercially available AVs is typically maintained with features such as automatic emergency braking [6] and lane keeping [7], where the longitudinal and lateral motion of the vehicle is controlled, respectively, based on the information from perception systems. A wide selection of onboard range sensors can be utilized for detection purposes, such as radar, lidar, and camera [8]. Additionally, recent advancements in communication technology have paved the way for wireless connectivity that provides reliable information exchange between different road users and the infrastructure. This, when integrated with AV technology, leads to connected automated vehicle (CAV) technology. Connectivity bears a substantial potential to amplify the above-mentioned prospects of AVs [9], [10], and some of these improvements have been reported in earlier experimental studies [11], [12], [13].

It is crucial to employ the right controller strategies to take full advantage of the benefits offered by the CAV technology. The control problem for a CAV usually consists of two main goals: optimizing the outcome of a desired prospect (such as minimizing energy consumption), and keeping the system safe (collision avoidance). The controller design for a CAV is often constructed in the context of optimization, for example, by finding the optimal parameters of a given controller obtained via classical control techniques [7] and data-driven methods [14], or by finding optimal trajectories for a finite horizon as in model predictive control (MPC) [15], [16], [17], [18]. MPC can potentially handle additional constraints to address the safety problem as well. However, its computational burden for solving complex nonlinear optimization problems in a rolling horizon fashion makes it challenging to be implemented in an on-board unit with limited computation capacity.

An alternative approach to satisfy both control tasks (performance and safety) is to focus on each problem separately and then integrate the resulting controller strategies in the implementation. Integration methods typically operate in the scheme of correcting (or interfering with) a performance-based controller according to a specific safety task. For example, the study [19] offers an adaptive cruise controller for longitudinal control with

Manuscript received 28 June 2023; revised 22 July 2023; accepted 9 August 2023. Date of publication 15 August 2023; date of current version 23 February 2024. This work was supported by Navistar Inc. (Corresponding author: Anil Alan.)

Anil Alan is with the Department of Mechanical Engineering, University of Michigan, Ann Arbor, MI 48109 USA (e-mail: anilalan@umich.edu).

Chaozhe R. He is with the Department of Mechanical Engineering, University of Michigan, Ann Arbor, MI 48109 USA, and also with the Plus.ai Inc., Santa Clara, CA 95014 USA (e-mail: chaozhe.he@plus.ai).

Tamas G. Molnar is with the Department of Mechanical and Civil Engineering, California Institute of Technology, Pasadena, CA 91125 USA (e-mail: tmolnar@caltech.edu).

Joahan Chacko Mathew is with the Visteon Corporation, Van Buren Township, MI 48111 USA (e-mail: jmathew2@visteon.com).

A. Harvey Bell is with the Multidisciplinary Design Program, University of Michigan, Ann Arbor, MI 48109 USA (e-mail: ahbelliv@umich.edu).

Gábor Orosz is with the Department of Mechanical Engineering, University of Michigan, Ann Arbor, MI 48109 USA, and also with the Department of Civil and Environmental Engineering, University of Michigan, Ann Arbor, MI 48109 USA (e-mail: orosz@umich.edu).

Color versions of one or more figures in this article are available at <https://doi.org/10.1109/TIV.2023.3305204>.

Digital Object Identifier 10.1109/TIV.2023.3305204

a switching structure: a nominal controller is switched to a braking trajectory when a prescribed minimum safe distance from the preceding vehicle is no longer satisfied. In [20], a command/reference governor method is utilized to adjust an existing higher-level controller to satisfy safety constraints over a horizon. Another scheme is proposed in [21], where formal methods guarantee safety specifications with a correct-by-construction controller, which can be used as a supervisor to interfere with an existing controller. Although shown effective, these integration strategies operate according to a certain safety condition that is calculated specifically based on the defined safety task. Therefore, these methods inherently lack the flexibility to employ *any* existing safety-oriented controller that can be preferable because it has been developed based on safety assessment methods [22] or because it has been exhaustively tested under real road conditions, often by external parties.

A method that can potentially eliminate this practical limitation is proposed in [23] for platoon control. This scheme selects the minimum of two desired accelerations that are designed separately to maintain an intended speed (speed control mode) and to keep a safe distance from the preceding vehicle (gap control mode). While it is intuitive, the authors do not provide a discussion on the safety implications of this approach. More importantly, the efficacy of the method has not been evaluated on an experimental platform. Instead, numerical simulations are used to validate the safety of the platoon.

In our work, we utilize the integration scheme of *selecting the minimum desired acceleration*, and we establish the connection between this scheme and the theoretical framework of control barrier functions [24]. Through this framework we provide formal safety guarantees for the controller integration scheme. Moreover, we propose a more general version of this type of controller integration: a safe integration method with a *safety filter* for longitudinal control of CAVs. Our method is more general in the sense that it is compatible with any types of safety-oriented controllers, e.g., those running on commercially available AVs, without requiring modifications to these controllers. We demonstrate the efficacy of our proposed safe integration scheme on a connected automated truck (CAT). The CAT is equipped with a cruise controller that uses connectivity to maintain a safe car following behavior (connected cruise controller—CCC) and a predictive-type performance-based controller that minimizes the energy input over a specified horizon by leveraging the gravitational potential energy (predictive cruise controller—PCC).

The proposed controller integration scheme is validated through hardware experiments with a full-scale CAT in different experimental scenarios. Proof-of-concept experiments are conducted in a fully-controlled environment on a closed test track. Through these experiments we show that safe driving is maintained thanks to the CCC, while energy savings up to 18% are obtained with the PCC. Next, we conduct experiments in a partially-controlled environment on a public highway. The measurements obtained from these highway experiments agree with the previous results: safe and seamless integration can be achieved through the proposed simple yet effective method—even in real traffic. Furthermore, we compare the results to a baseline algorithm that switches between the PCC and the CCC

based on the time headway. It is shown that comparable energy-saving percentages and smooth driving may not be obtained if one does not design the integration carefully.

The organization of the article is as follows. In Section II, we give a detailed description of the driving scenarios with a CAT, and we present models representing the system. In Section III, we first introduce the general safe integration scheme for the longitudinal control problem of CAVs. Then, we describe the design steps of an energy optimal nominal controller (PCC) and a safety-oriented controller (CCC) for CATs. Section IV presents our on-track experimental results validating the proposed controller structures separately as well as their integration through the proposed scheme. In this section we also compare our findings with a naive switching algorithm. We present experimental results on a public highway in Section V and conclude the article in Section VI.

II. SYSTEM DESCRIPTION AND MODELING

Here we describe the driving scenario and the truck's sensor and control systems. Then we give dynamical models representing the system.

A. System Description

This study considers a scenario where a CAT drives on a highway with changing elevation. The CAT either drives with no influence from the preceding traffic, as shown in Fig. 1(a), or it follows a preceding vehicle, as in Fig. 1(b) and (c). Onboard the CAT, there is a range sensor for detecting preceding vehicles and a communication module that enables connectivity with other connected vehicles (CVs). We consider scenarios with one CV ahead, but the proposed controller scheme can be extended to multiple CVs. The vehicle immediately in front of the CAT may be the CV, as shown in Fig. 1(b), or there may be other non-connected vehicles (nCVs) in between the CAT and CV, as in Fig. 1(c).

Our goal is to control the longitudinal motion of the CAT based on the information from the range sensor and communication module. We want to maintain safety as the primary concern while attaining the desired driving performance when possible. In this study, we consider the energy efficiency as the performance criterion. To achieve our goal, we implement the control system illustrated in the block diagram in Fig. 2. We retrofit the CAT with drive-by-wire actuators, which control the powertrain and brake subsystems based on the driver's pedal inputs [25]. We intervene the drive-by-wire system by replacing the driver's inputs with the *desired pedal positions* calculated by a proposed longitudinal controller.

The longitudinal controller we implement consists of a two-layer architecture with high and low levels. The high-level controller calculates the *desired longitudinal acceleration*, denoted by u , based on a high-level controller goal. The high-level controller block in Fig. 2 highlights some examples of these controllers and a safe integration scheme called a safety filter, which will be detailed in Section III.

The low-level controller finds the corresponding desired pedal commands to track the desired acceleration commands

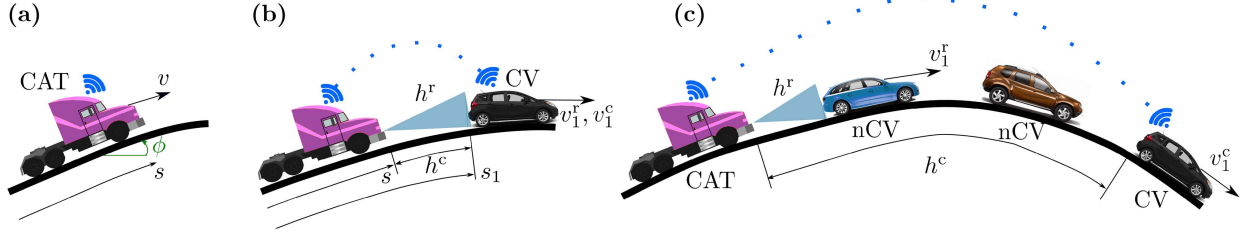


Fig. 1. Connected automated truck (CAT) driving on a highway in three scenarios. (a) There is no preceding vehicle. (b) The closest preceding vehicle is a connected vehicle (CV) detected by the range sensor and connectivity simultaneously. (c) There are non-connected vehicles (nCVs) between the CAT and the CV, and range sensor and connectivity detect different vehicles.

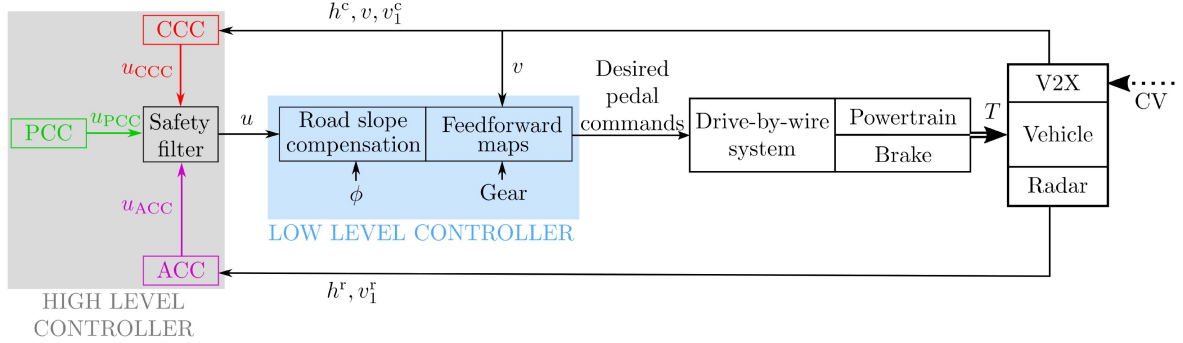


Fig. 2. Block diagram representing the control architecture implemented on the connected automated truck.

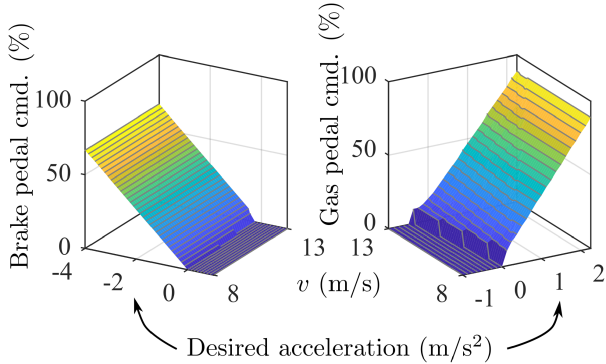


Fig. 3. Feedforward maps utilized by the low-level controller outputting the pedal positions to track the desired acceleration commands. The right panel shows the map for gear 7.

as closely as possible. Specifically, the low-level controller uses experimental data containing the acceleration response to pedal commands. These data were generated at various speed levels, gears, and pedal commands in an open-loop fashion. The resulting relationships are inversely encoded in the low-level controller as feedforward maps, which give the corresponding pedal commands to achieve the commanded acceleration based on speed and gear. For example, Fig. 3 depicts the feedforward maps utilized in gear 7. Note that the experimental data used in the feedforward map calculations do not capture the effect of the road slope. Thus, we compensate for the gravitational effect before applying the feedforward maps using road slope information obtained from elevation data. These data were collected via GPS along the particular road sections utilized prior to performing the experiments.

The control system relies on sensory information from the communication module and from the range sensor to calculate the high-level acceleration command. The communication module can measure GPS coordinates, and the ground speed v of the CAT. It also receives information from the CV, including its ground speed v_1^c and GPS coordinates. These coordinates are used to calculate the longitudinal bumper-to-bumper headway h^c between two vehicles [12]. The range sensor is mounted on the front bumper and measures the headway h^r between the closest preceding vehicle and the CAT. It also measures the relative speed between vehicles, which is added to v to get the ground speed v_1^r of the preceding vehicle. For simplicity, we will drop the superscripts ‘c’ and ‘r’ when there is no ambiguity and use them only to emphasize the difference between the source of the data (connectivity or range sensor) when needed.

B. Modeling

Here, we introduce the system models utilized for control design. First principles are used to derive the longitudinal vehicle dynamics for a rear-axle-driven truck without headwind [27]:

$$\begin{aligned} \dot{s} &= v, \\ \dot{v} &= \frac{T_w}{Rm_{\text{eff}}} - \underbrace{\frac{mg}{m_{\text{eff}}} (\sin(\phi(s)) + \gamma \cos(\phi(s)))}_{f_1(\phi(s))} - \underbrace{\frac{k_{\text{air}}}{m_{\text{eff}}} v^2}_{f_2(v)}, \end{aligned} \quad (1)$$

where s is the distance traveled by the front bumper of the CAT along the road, v and \dot{v} are the longitudinal speed and acceleration, and $\phi(s)$ is the road slope changing along the road;

TABLE I
CAT PARAMETERS USED IN THIS STUDY CORRESPONDING TO A 2011
INTERNATIONAL PROSTAR+ CLASS-8 TRUCK MANUFACTURED BY NAVISTAR
CORPORATION [26]

R	0.5 m	m	9000 kg	m_{eff}	9157 kg
γ	0.006	k_{air}	3.84 kg/m	g	9.81 m/s ²
\underline{u}	4 m/s ²	\bar{u}	2 m/s ²	\bar{P}	93 kW

see Fig. 1(a). Parameters in the model are the tire radius R , truck mass m , effective mass $m_{\text{eff}} = m + I/R^2$ (incorporating the mass moment of inertia I of rotating elements), rolling resistance γ , air drag coefficient k_{air} , and gravitational acceleration g . For this study we use parameters corresponding to a truck without a trailer, given in Table I.

Here T_w denotes the net wheel torque applied at the rear axle, consisting of a positive driving and a negative braking component. To work with these components using units of acceleration for convenience, we utilize the conversion $T_w = \hat{u}Rm_{\text{eff}}$ and reformulate (1) as

$$\dot{s} = v, \quad \dot{v} = \hat{u} - f_1(\phi(s)) - f_2(v). \quad (2)$$

We remark that the scaled torque input \hat{u} can be split as

$$\hat{u} = u_{\text{dr}} + u_{\text{br}}, \quad (3)$$

where $u_{\text{dr}} \geq 0$ and $u_{\text{br}} \leq 0$ represent the scaled driving and braking torques, respectively. This will be utilized when constructing the performance-based controller further below. Assuming that the low-level controller ideally compensates the functions f_1 and f_2 , the model (2) reduces to

$$\dot{s} = v, \quad \dot{v} = u, \quad (4)$$

where u represents the desired acceleration prescribed by the high-level controller.

We describe the motion of preceding vehicles using the kinematic model:

$$\dot{s}_1 = v_1, \quad \dot{v}_1 = a_1, \quad (5)$$

where s_1 is the distance traveled by the rear bumper of the preceding vehicle in consideration (see Fig. 1(b) and (c)), while v_1 and a_1 denote the corresponding speed and acceleration. To utilize the distance headway in the high-level controller we first define the variable $h \triangleq s_1 - s$, and use (4) and (5) to obtain the car-following model:

$$\dot{h} = v_1 - v, \quad \dot{v} = u, \quad \dot{v}_1 = a_1. \quad (6)$$

Whether the preceding vehicle in consideration is a CV or a nCV, we may add the superscripts ‘c’ and ‘r’ for h and v_1 to highlight the feedback’s source; see Fig. 1(b) and (c).

In order to take into account the physical limitations in the powertrain and brake we limit the desired acceleration:

$$-\underline{u} \leq u \leq \min \left\{ \bar{u}, \frac{\bar{P}}{m_{\text{eff}} v} \right\}. \quad (7)$$

Here \underline{u} is the maximum deceleration limit corresponding to the maximum brake torque. The term \bar{u} denotes the maximum acceleration corresponding to the maximum torque applied on

the driven wheels. The desired acceleration is also limited by the maximum power \bar{P} of the powertrain. We list the values of \underline{u} , \bar{u} , and \bar{P} in Table I. Finally, we also consider

$$\underline{v} \leq v \leq \bar{v}, \quad (8)$$

where the speed limits \underline{v} and \bar{v} are determined based on the road curvature, surface conditions, and legal limitations.

III. CONTROLLER DESIGN

In this section we formally define safety for a connected automated vehicle in the single-lane scenario. We introduce the notion of a safety filter based on the safety-critical control task. Then, we show the design steps for a safety-oriented connected cruise controller and an optimal-in-energy nominal controller for a connected automated truck.

A. Safe Controller Integration Scheme

The safety task for a CAV within a single lane (i.e., no overtaking considered) is to follow the preceding vehicle while maintaining *at least* a certain critical distance at all times. This can be formulated as

$$h(t) \geq \rho(v(t), v_1(t)), \quad \forall t \geq 0, \quad (9)$$

where the function ρ gives the critical distance based on the speeds of the CAV and the preceding vehicle.

There are many possible approaches to specify the critical distance ρ , such as the minimum time-to-collision [28] or minimum time headway [29]. Furthermore, one may take the input capabilities of the CAV, given by (7), into consideration to provide feasibility to the resulting safety-critical controller as described in [30], which is then extended to a smooth quadratic function in [31]. The scheme proposed in this study can be applied to a large class of safety tasks under Assumption 1.

Assumption 1: The critical distance the CAV shall keep from the preceding vehicle strictly increases with the speed of the ego vehicle; that is, for a continuously differentiable ρ we have

$$\frac{\partial}{\partial v} \rho(v, v_1) > 0, \quad (10)$$

for all $v \in [\underline{v}, \bar{v}]$ and $v_1 \geq 0$.

The reasoning behind this assumption is that the faster the vehicle travels, the larger distance it shall keep.

Safety tasks in the form of (9) are often studied in the context of *set invariance* in the literature [32], where the state of a dynamical system should remain inside a prescribed set for all time. To be specific, consider a set given as

$$\mathcal{C} \triangleq \{[h, v, v_1]^\top \in \mathbb{R}^3 \mid h - \rho(v, v_1) \geq 0\}, \quad (11)$$

for the car-following setup (6). For an initial condition $[h(0), v(0), v_1(0)]^\top \in \mathcal{C}$, if $[h(t), v(t), v_1(t)]^\top \in \mathcal{C}$ for all $t \geq 0$, then we say the system is *safe* with respect to the set \mathcal{C} , which ensures safety defined as (9).

Control barrier functions (CBFs) offer a solution to synthesize controllers for problems of this type [24]. A detailed description is given in Appendix A. In simple terms, a CBF renders a system safe by providing a condition for the controller to

satisfy (cf. (32)). When this condition is used as a constraint to modify a nominal control input to the closest safe input (cf. (33)), the resulting controller is called *safety filter*. Safety filters operate instantaneously (without any horizon) and offer easy-to-implement solutions, especially for single input systems such as the longitudinal control of a CAV.

We use the model (6) for a general CAV, which, along with Assumption 1, yields the CBF-based safety filter

$$u = \min \{u_{\text{nom}}, u_{\text{safe}}\}, \quad (12)$$

see Appendix A for calculation details. This algorithm will be used as the proposed *safe controller integration scheme*. Here u_{nom} is a nominal controller that can be tailored to optimize an aspect of the system without considering safety, such as optimal-in-energy driving. The term u_{safe} denotes a safety-critical controller, which can be any algorithm certified to keep the system safe by satisfying the controller constraint provided by the CBF. When the nominal controller gives smaller input than the safety-critical controller, it can be shown to satisfy the safety task (9). Therefore, the safety filter passes the nominal controller without modification to maintain performance. However, the safety filter switches to the safety-critical controller when its input becomes smaller than the nominal one to ensure that safety is not violated.

In the remainder of this section, we present details about implementing the safe controller integration scheme (12) to the longitudinal control problem of a connected automated truck with a safety-critical controller and an energy-efficient nominal controller. We note that CBFs can also provide us with a form of u_{safe} (cf. (35)) for a specific selection of ρ used in the safety task (9). However, since we do not specify ρ , we choose to replace the CBF-based safety-critical controller with another safety-oriented controller shown to be safe experimentally under various working conditions.

B. Safety-Oriented Connected Cruise Controller

A connected cruise controller structure is utilized as the safety-oriented controller for the safety filter (12). This type of controller was studied extensively for stability and string stability under time delays and system uncertainties [33], [34], [35], and it was shown to be safe experimentally for different driver behaviors [12].

The controller structure is given as

$$u_{\text{safe}}(h, v, v_1) = A(h)(V(h) - v) + B(h)(W(v_1) - v), \quad (13)$$

where the first term gives the desired acceleration based on the speed error associated with the *range policy*

$$V(h) = \begin{cases} 0 & \text{if } h \leq h_{\text{st}}, \\ \kappa(h - h_{\text{st}}) & \text{if } h_{\text{st}} < h < h_{\text{go}}, \\ \bar{v} & \text{if } h \geq h_{\text{go}}, \end{cases} \quad (14)$$

see Fig. 4(a). Parameter h_{st} denotes the stopping distance, and κ is the gradient determining the relationship between the distance headway and the target speed. The value $h_{\text{go}} \triangleq h_{\text{st}} + \bar{v}/\kappa$ is the distance, after which the range policy outputs the maximum

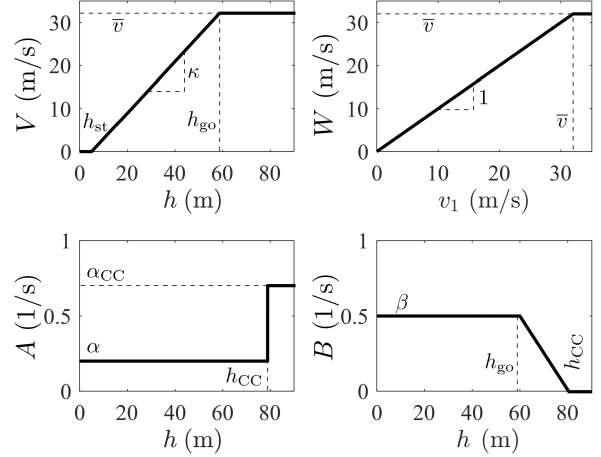


Fig. 4. Range policy (14), speed policy (15), controller gain functions (16) and (17) with parameters used in Section V.

speed \bar{v} as the target speed. The second term in (13) yields the desired acceleration based on the relative speed subject to the *speed policy*

$$W(v_1) = \min \{v_1, \bar{v}\}, \quad (15)$$

which is introduced to put a bound on the speed error in case the preceding vehicle moves faster than the speed limit, see Fig. 4(b).

Terms A and B determine the gains associated with the speed errors based on the range policy and the relative speed. We choose

$$A(h) = \begin{cases} \alpha & \text{if } h \leq h_{\text{CC}}, \\ \alpha_{\text{CC}} & \text{if } h > h_{\text{CC}}, \end{cases} \quad (16)$$

$$B(h) = \begin{cases} \beta & \text{if } h \leq h_{\text{go}}, \\ \beta \frac{h_{\text{CC}} - h}{h_{\text{CC}} - h_{\text{go}}} & \text{if } h_{\text{go}} < h < h_{\text{CC}}, \\ 0 & \text{if } h \geq h_{\text{CC}}, \end{cases} \quad (17)$$

as depicted in Fig. 4(c) and (d). Notice that the effect of the preceding vehicle's speed gradually diminishes for larger headways. For $h \geq h_{\text{CC}}$ we have $A(h) = \alpha_{\text{CC}}$ and $B(h) = 0$, that is, (13) yields the constant speed cruise controller $\alpha_{\text{CC}}(\bar{v} - v)$ tracking the maximum speed \bar{v} with a constant gain α_{CC} . We will specify the distance $\delta \triangleq h_{\text{CC}} - h_{\text{go}}$ in the experiments discussed further below.

We remark that given a specific selection of a differentiable function ρ , one may potentially show that the controller (13) certifies the safety of the set \mathcal{C} defined in (11) by satisfying (32) for a large enough h_{st} and small enough κ .

C. Performance-Based Nominal Controller

We consider the 'wheels-to-distance' energy efficiency as the performance aspect of a truck [36], and we employ a *predictive cruise controller (PCC)* [37]. PCC minimizes the mechanical energy input by taking the constraints on powertrain output and speed (7) and (8) into account and by taking advantage of the variable road slope over a preview distance $s \in [0, s_f]$, where s_f denotes the end of the horizon.

In PCC, we formulate an optimal control framework to find the optimal drive and brake components u_{dr}^* and u_{br}^* in (3) while minimizing the mechanical energy. The vehicle model (2) is used as a constraint in the optimal control framework. Since the road slope depends on the position, i.e., $\phi(s)$, the implementation variables are converted from the time domain to spatial domain using $\frac{dt}{ds} = \frac{1}{v}$ while assuming positive speed:

$$0 < \underline{v} \leq v \leq \bar{v}, \quad (18)$$

cf. (8). These lead to the model

$$\frac{dv}{ds} = \frac{u_{\text{dr}} + u_{\text{br}}}{v} - \frac{f_1(\phi(s)) + f_2(v)}{v}. \quad (19)$$

Similar to (7) we consider the following limitations on decision variables:

$$0 \leq u_{\text{dr}} \leq \min \left\{ \bar{u}_{\text{dr}}, \frac{\bar{P}}{m_{\text{eff}} v} \right\}, \quad (20)$$

$$-u_{\text{br}} \leq u_{\text{br}} \leq 0, \quad (21)$$

$$u_{\text{dr}} u_{\text{br}} = 0, \quad (22)$$

where $\underline{u}_{\text{br}}$ and \bar{u}_{dr} correspond to the maximum driving and braking torques, and \bar{P} denotes the maximum power of the powertrain. The constraint (22) is introduced to ensure that throttle and brake are not active simultaneously.

The cost function we wish to minimize is selected as the mechanical energy input per unit effective mass:

$$w(t) = \int_0^t u_{\text{dr}} v \, d\tilde{t}, \quad (23)$$

where the integrand refers to the power input per unit effective mass. Note that we do not include the brake torque component in (23) to prevent possible negative consumption when brakes are active.

Converting the energy integral to the spatial domain (18)–(23) result in the optimal control problem [37]:

$$\begin{aligned} (u_{\text{dr}}^*, u_{\text{br}}^*) &= \underset{(u_{\text{dr}}, u_{\text{br}}) \in \mathbb{R}^2}{\operatorname{argmin}} \int_0^{s_f} u_{\text{dr}} \, ds, \\ \text{subject to } \frac{dv}{ds} &= \frac{u_{\text{dr}} + u_{\text{br}}}{v} - \frac{f_1(\phi(s)) + f_2(v)}{v}, \\ 0 &\leq u_{\text{dr}} \leq \min \left\{ \bar{u}_{\text{dr}}, \frac{\bar{P}}{m_{\text{eff}} v} \right\}, \\ -u_{\text{br}} &\leq u_{\text{br}} \leq 0, \\ u_{\text{dr}} u_{\text{br}} &= 0, \\ \underline{v} &\leq v \leq \bar{v}, \\ v(0) &= v_0, \\ v(s_f) &= v_f, \\ \int_0^{s_f} \frac{1}{v(s)} \, ds &\leq \bar{t}_f, \end{aligned} \quad (24)$$

with boundary conditions $v(0) = v_0$ and $v(s_f) = v_f$ for speed. The last constraint with maximum travel time \bar{t}_f is introduced to ensure that the travel time is not sacrificed for better energy

efficiency. We typically obtain boundary conditions and the maximum travel time from a benchmark run driven by an expert human driver.

To solve the optimization problem (24), we rely on road slope data obtained as follows. We use GPS measurements of the benchmark run to calculate the discretized travel distance values s_i along the road. The slope, $\phi(s_i) = \sin^{-1}(\frac{dE(s_i)}{ds})$, is calculated from the elevation $E(s_i)$ measured at corresponding points s_i via numerical differentiation. Finally, the open-source interior point solver IPOPT [38] is used to solve the resulting nonlinear programming problem offline, yielding the optimal inputs $u_{\text{dr}}^*(s_i)$ and $u_{\text{br}}^*(s_i)$ as well as the optimal speed profile $v_{\text{PCC}}^*(s_i)$. Rather than directly implementing the optimal inputs, we employ a feedback controller strategy to reject potential disturbances emerging from the inaccuracies in the low-level controller. Thus, a variable-speed cruise controller with a constant gain α_{CC} is implemented:

$$u_{\text{PCC}}(s, v) = \alpha_{\text{CC}} (v_{\text{PCC}}(s) - v), \quad (25)$$

where $v_{\text{PCC}}(s)$ is calculated from $v_{\text{PCC}}^*(s_i)$ via interpolation for any given $s \in [0, s_f]$.

Energy efficiency evaluation for different experimental runs is carried out by calculating the cost function (23) along the road. Since we do not implement u_{dr}^* directly, we need to calculate the u_{dr} values corresponding to the implemented controller effort. We calculate u_{dr} using the vehicle dynamics (2) and the measured speed, acceleration, and road slope data:

$$u_{\text{dr}} = \max \{0, \dot{v} + f_1(\phi(s)) + f_2(v)\}, \quad (26)$$

where $\max\{0, \cdot\}$ is introduced to ensure $u_{\text{dr}} \geq 0$.

D. Implemented Safe Controller Integration Scheme for CAT

Having introduced controller strategies (13) and (25) based on different tasks, we now integrate them using the safety filter concept (12). Utilizing the structure (13), we employ two safety-oriented controllers distinguished by their feedback source. We name the controller $u_{\text{safe}}(h^r, v, v_1^r)$, which relies on the range sensor data, as the adaptive cruise controller (ACC) and denote it by u_{ACC} . The controller $u_{\text{safe}}(h^c, v, v_1^c)$, which employs the connectivity-based data, is called the connected cruise controller (CCC) and is denoted by u_{CCC} . The nominal controller is selected as PCC (25), yielding:

$$\begin{aligned} u(s, h^c, h^r, v, v_1^c, v_1^r) &= \min \{u_{\text{ACC}}(h^r, v, v_1^r), \\ &u_{\text{CCC}}(h^c, v, v_1^c), \\ &u_{\text{PCC}}(s, v)\}, \end{aligned} \quad (27)$$

see Fig. 2. In (27), PCC is utilized as long as it is considered as safe, and switch to either of the safety-oriented controllers occurs based on their feedback.

It is noted that the CV detected through connectivity may or may not be the closest preceding vehicle in open traffic, as shown in Fig. 1(b) and (c). If the CV is the closest preceding vehicle, ACC and CCC respond to the same vehicle (with slight differences based on sensor readings). When other non-connected vehicles are between the CAT and CV, the range sensor detects

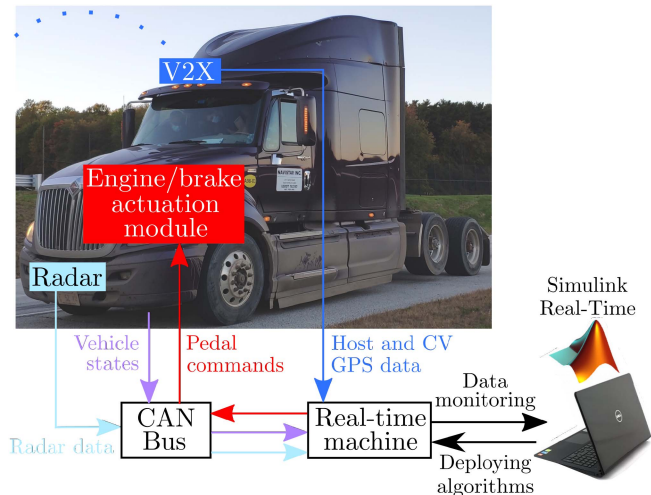


Fig. 5. Connected automated truck (CAT) used for experiments and the information flow between its units.

the closest preceding vehicle and ACC responds accordingly, while CCC follows the CV. In this specific scenario, CCC becomes redundant. Yet, we remark that the beyond-line-of-sight detection capabilities of the connectivity forebode significant improvement in both safety and energy efficiency [10], [39], [40]. In this study, we focus on proving the efficacy of the proposed safe controller integration method. Thus we leave the work of utilizing more sophisticated connectivity-based controller structures as future work.

IV. ON-TRACK EXPERIMENTS

In this section, we describe the experimental results obtained on a closed track to validate the proposed controller structures. In these experiments, the CAT was controlled to follow an optimal-in-energy speed profile without a preceding vehicle, or to follow a preceding CV according to the scenarios depicted in Fig. 1(a) and (b). After describing the experimental setup and procedure, the results for the nominal controller, the safety-oriented controller, and the integrated controller with the proposed safety filter scheme are introduced.

A. Details About Experimental Setup and Procedure

We used a 2011 International ProStar+ Class-8 truck developed by Navistar [26] as the CAT; see Fig. 5. The truck has engine and brake actuation modules configured to follow the desired pedal commands sent through the vehicle-CAN bus following J1939 CAN protocol [41]. The vehicle states, such as the wheel speed, gear position, engine torque and rpm, and brake pressure are also available on the CAN bus under the same protocol. The truck is equipped with a Mobile Real-Time Targeting Machine developed by Speedgoat [42], which reads the vehicle states from the vehicle-CAN bus, runs the control algorithms in Simulink Real-Time, computes the corresponding desired pedal commands, and sends them to the vehicle-CAN bus. A personal computer was connected to the real-time machine deploying algorithms in one direction and monitoring data in another. The

TABLE II
CONTROLLER PARAMETERS USED FOR ON-TRACK EXPERIMENTS

h_{st}	5 m	κ	0.6 1/s	δ	20 m
α	0.4 1/s	β	0.5 1/s	α_{CC}	0.9 1/s
\bar{u}_{dr}	2 m/s ²	\underline{u}_{br}	4 m/s ²	\underline{v}	2.5 m/s

computer could also abort the mission at any time, giving the control for pedals back to a human driver. Steering was carried out by an expert human driver all the time.

A radar was utilized as the range sensor. The radar sent messages containing the headway and relative speed information belonging to the closest preceding vehicle to the vehicle-CAN bus. Both the truck and the CV were equipped with a vehicle-to-everything (V2X) communication onboard unit (OBU) developed by Commsignia [43]. These units provide GPS coordinates and GPS-based speed measurements and support peer-to-peer communication between vehicles. The V2X OBU on the truck received data packets broadcasted by the CV's V2X OBU at a rate of 10 Hz, containing GPS coordinates and speed information of the CV. The real-time communication between the CAT's V2X OBU and the Speedgoat was established using user datagram protocol (UDP).

The on-track experiments were conducted at Navistar Proving Grounds, a test track closed to the public in New Carlisle, Indiana, USA. The route used is shown in Fig. 6(a) with the GPS trace of a benchmark run (red loop in the clockwise direction). The start-end point of the experiments is marked by a green triangle. Using GPS-based elevation measurements from multiple benchmark runs, an average elevation profile of the track was estimated as shown in Fig. 6(b). Blue triangles on the map and the elevation plot indicate sharp turns; these were considered when designing the speed limit \bar{v} for that particular part of the road, see the black dashed line in Fig. 6(c). We also used a smaller speed limit in the middle section due to poor road surface quality.

The loop of nearly 3000 meters of length was discretized using the GPS trace of a benchmark run, resulting in GPS data points approximately 2.5 meters away from each other. The optimal control problem (24) was solved offline, and the corresponding optimal-in-energy speed profile v_{PCC} is plotted in Fig. 6(c) as a gray dotted curve. The resulting energy consumption per unit effective mass (23), i.e., the cost function in (24), is depicted in Fig. 6(d) as a gray dotted curve. Notice that the optimal profile requires very little energy after 1800 m and utilizes the gravitational potential energy to finish the drive while obeying the speed limit. We used parameters given in Table II for all the on-track experiments detailed in this section.

B. Results

First, we implemented the PCC controller (25) on the CAT without any preceding vehicle on the track. The results are depicted in Fig. 6(c) as a green curve. One may observe good speed-tracking performance in the cruise control, which verifies the performance of the low-level controller. The corresponding energy consumption per unit mass calculated from (23) is shown

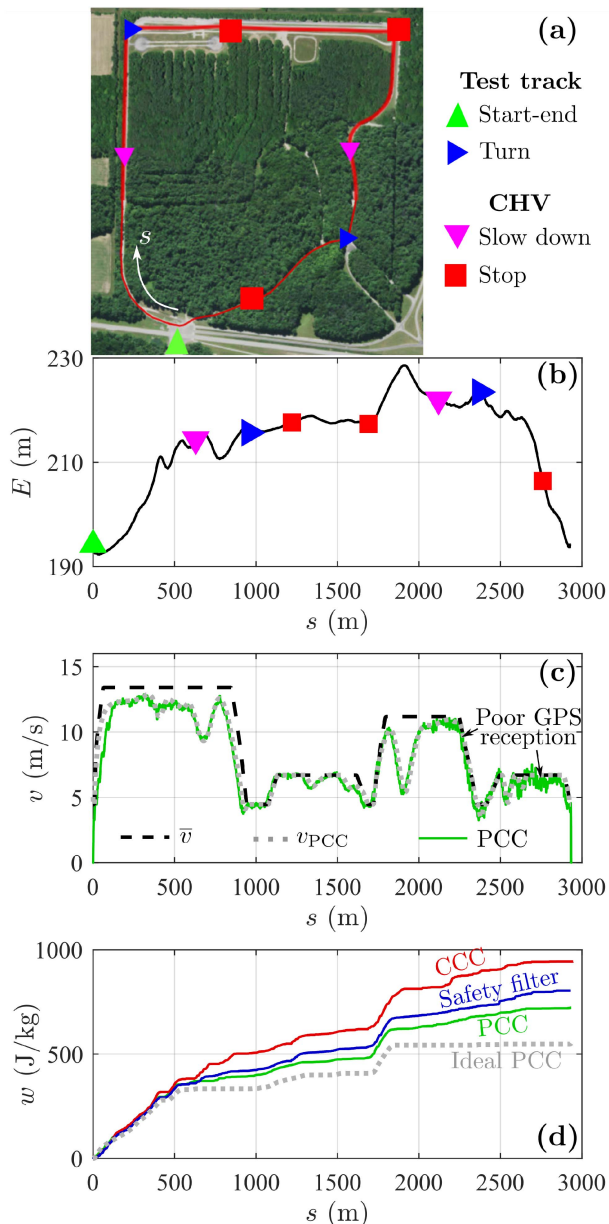


Fig. 6. (a) Test track used for experiments with landmarks indicating details about the CV speed profile design. (b) Elevation profile E with corresponding landmark positions. (c) Speed limit \bar{v} , optimal-in-energy speed profile v_{PCC} , and measured speed profile v in the PCC experiments. (d) Energy consumption curves w calculated from experimental data using (23) for different controllers.

in Fig. 6(d) as a green curve. One may notice the difference between the ideal energy consumption (gray dotted curve) and the experimental one (green curve). This gap is partly due to the powertrain dynamics omitted in the optimal control problem (24), and partly due to the noise in the experimental data, especially towards the end of the run. This noise was due to poor GPS reception, caused by a dense canopy, and it was amplified by the numerical differentiation employed to obtain the acceleration in (26). When integrated per (23), the noise results in a positive drift due to the function $\max\{0, \cdot\}$. Since we employ a comparative analysis among different controller runs in this study, we ignore these imperfections and focus on how well a controller performs

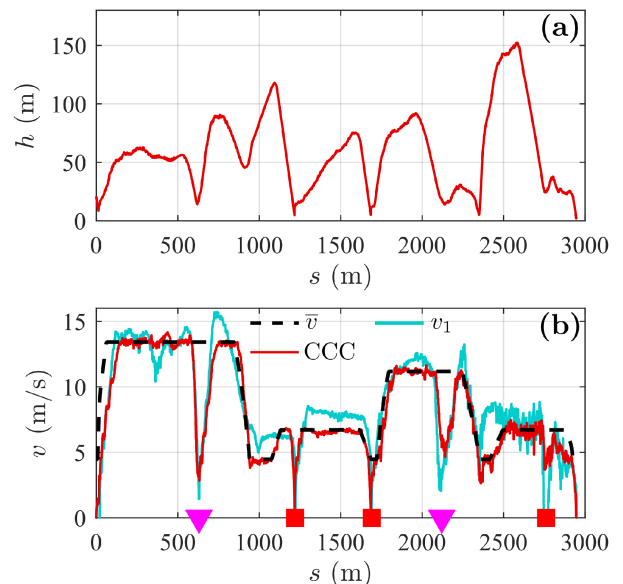


Fig. 7. Experimental results from a CCC run. (a) Measured distance headway h . (b) Speed limit \bar{v} , CV speed profile v_1 , and measured CAT speed profile v in the experiment.

in terms of energy consumption compared to other controllers in the experiments.

Next, we experimentally validated the safety-oriented controller (13) such that the CAT traveled behind a CV. Since the test track was closed to public traffic and no non-connected vehicles were present, we only implemented CCC utilizing connectivity-based data. This setup, which is equivalent to the radar-based ACC in this scenario as depicted in Fig. 1(b), allowed us to record the GPS trace and speed of the CV in a particular run and later re-play this record for the CAT. These experiments not only prevented a physical collision in the case of a malfunction in hardware or software but also provided us with consistent preceding vehicle motion across different runs so that the repeatability could be evaluated solely on the merits of controllers. In particular, we designed a speed profile v_1 for the preceding vehicle that imitates a heavy traffic scenario with multiple slowdowns (marked by magenta triangles) and stops (marked by red squares). Fig. 7(b) shows the resulting CV speed profile as a cyan curve.

Experimental results for a CCC run are given in Fig. 7, where panel (a) shows the measured distance headway and panel (b) depicts the measured speed, both as red curves. CCC keeps the system safe by maintaining a positive headway throughout the run. Moreover, the truck successfully obeys the speed limit even when the CV moves faster than the limit. The energy consumption throughout the run is depicted in Fig. 6(d) as a red curve, where the car-following is observed to yield significantly more energy input rates than PCC around 700 meters and around 1800 meters due to the braking and acceleration maneuvers triggered by the CV's motion.

Finally, we implemented the safety filter (27) utilizing the PCC and CCC as nominal and safety-oriented controllers (without the radar-based ACC). Results are given in Fig. 8, where

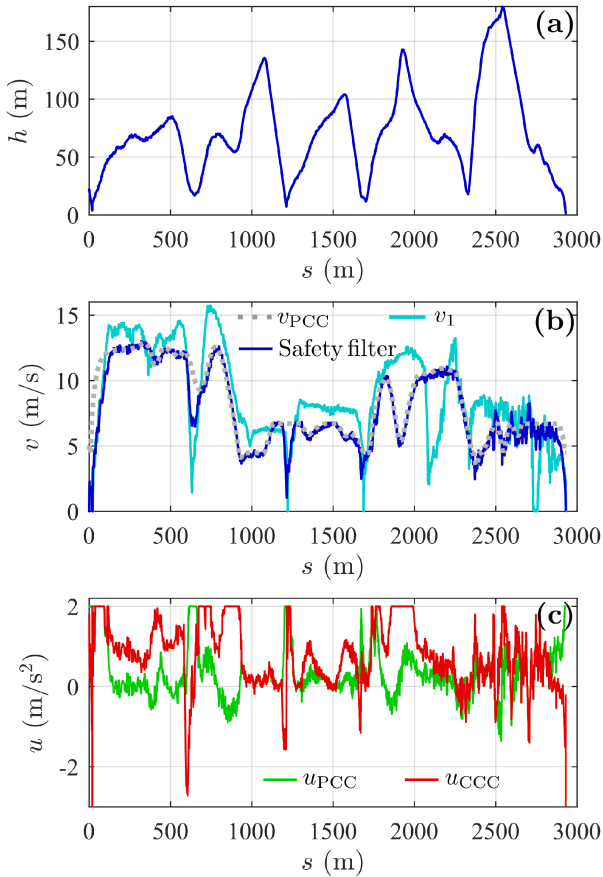


Fig. 8. Experimental results while applying the proposed safe controller integration scheme. (a) Measured distance headway h . (b) CV speed profile v_1 , optimal-in-energy speed profile v_{PCC} , and measured CAT speed profile v in the experiment. (d) Controller outputs u_{PCC} and u_{CCC} . The safety filter passed the minimum of these.

panel (a) shows the measured distance headway and panel (b) depicts the measured speed, both as blue curves. Panel (c) displays controllers u_{PCC} and u_{CCC} as green and red curves, respectively. Similar to the previously presented CCC result, a positive headway was maintained throughout the run thanks to the safety filter switching to CCC in critical moments around 600 m, 1200 m, and 1650 m. In these moments, the acceleration command of the CCC becomes smaller than that of the PCC, responding to the other vehicle and ensuring safety. At other times PCC was active since it suggested more energy-efficient driving rather than following the preceding vehicle.

We repeated these experiments 8–10 times for each configuration with same conditions (same CV speed profile was played back). Energy efficiency results are summarized in Table III under the label ‘Recorded’ in terms of energy saving values compared to the average of all CCC runs. In these runs PCC achieved 23% energy saving on average compared to the CCC, yet all of the PCC experiments were conducted on free driving scenario without any preceding traffic. The integration of the PCC and CCC through the safety filter yielded slightly less energy saving (18% compared to the CCC on average), yet the safety was established in all runs (headway never became negative).

TABLE III
SUMMARY OF ENERGY EFFICIENCY IN MULTIPLE EXPERIMENTS CONDUCTED USING A RECORDED CV SPEED PROFILE (CYAN CURVE IN FIG. 7(B)) AND A PHYSICAL (LIVE) CV REENACTING THE SAME PROFILE

CV data	Controller	Energy saving compared to CCC
Recorded	PCC	23% \pm 4%
	Safety Filter	18% \pm 3%
Live	PCC	25% \pm 4%
	Safety Filter	18% \pm 5%

Next, to evaluate the robustness of the method to the human-related variations, experiments were conducted with a physical human-driven preceding vehicle reenacting the CV speed profile v_1 with close accuracy. Same as in the previous experiments, the headway never reached zero in any of the CCC and safety filter runs. Moreover, similar energy efficiency results were obtained with a slight increase in the standard deviations, see results given in Table III under the label ‘Live’. This increase is due to the small variation between the speed profiles of the recorded CV and the human-driven CV. A video illustratively summarizing on-track experiments is available online [44].

C. Comparison to a Time Headway-Based Switch

The efficacy of the safe controller integration scheme is demonstrated via on-track experiments shown above. Here, we compare the proposed scheme to a baseline integration method (referred as the ‘naive switch’) that switches between the PCC and CCC based on the time headway.

The switching scheme is summarized as

$$u(s, h, v, v_1) = \begin{cases} u_{CCC}(h, v, v_1) & \text{if } h \leq \tau_{sw}v + h_{sw}, \\ u_{PCC}(s, v) & \text{if } h > \tau_{sw}v + h_{sw}, \end{cases} \quad (28)$$

where h_{sw} is the zero-velocity distance offset and $\tau_{sw} > 0$ is the critical time headway at which we make the switch. We fixed the parameter $h_{sw} = 10$ m, and repeated the on-track experiments with the same recorded preceding vehicle profile, depicted in Fig. 7(b), using different critical time headway values from the set $\tau_{sw} \in \{2, 4, 6, 8\}$ seconds. Experiments were repeated 3 times for each parameter set. The average and standard deviation of the final energy consumption values are given in Fig. 9(a) along with other controller runs. Energy consumption values for the naive switch runs span the gap between the safety filter runs and the CCC runs, where smaller τ_{sw} yields less consumption. This is expected because a smaller τ_{sw} increases the time that PCC is active.

While the proposed integration scheme resulted in smooth transitions between PCC and CCC (due to the Lipschitz continuity guaranteed by control barrier function theory), the naive switch typically led to abrupt jumps in the control input. The average of the absolute values of all jumps in the control input (i.e., $|\Delta u(t_k)| \triangleq |u(t_k) - u(t_{k-1})|$ at switching times t_k) is shown in Fig. 9(b). While the seamless integration via the safety filter led to $|\Delta u|$ values close to zero, the naive switch yielded large jumps and uncomfortable driving, especially for smaller

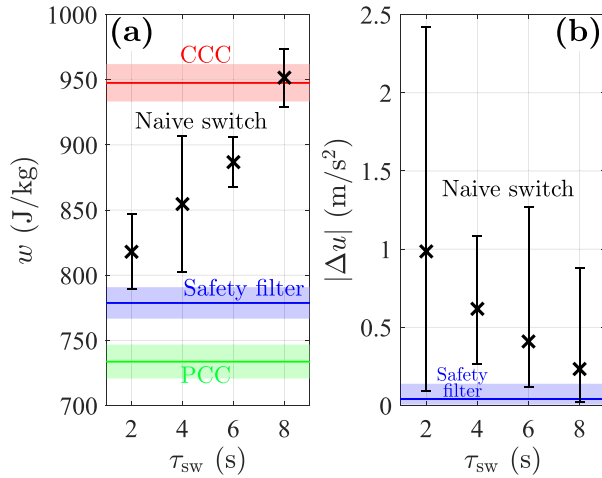


Fig. 9. (a) Average and standard deviation of the final energy consumption w in all ‘recorded’ runs. The energy consumption values decrease for the naive switch (28) as critical time headway τ_{sw} decreases. (b) Average and standard deviation of the jumps $|\Delta u|$ in the controller command at the switches between PCC and CCC. The naive switch is discontinuous, and decreasing τ_{sw} yields more abrupt changes in the command. The proposed safety filter-based controller integration scheme (27) is inherently continuous and provides smooth driving.

τ_{sw} . We note that the positively skewed distribution of $|\Delta u|$ leads to asymmetric deviations depicted with asymmetric error bars in Fig. 9(b).

V. HIGHWAY EXPERIMENTS

Having proved the efficacy of the safety filter in a closed test track, we proceed to validate the proposed structure on a public highway.

A. Details About the Experimental Procedure

In these experiments, the CAT was driven on a public road amongst non-connected human-driven vehicles (nCVs), and one connected vehicle (CV) was driven by an expert driver from our team. Thus, scenarios in both Fig. 1(b) and (c) occurred. For the CAT, we used the same experimental setup as described in the previous section; see Fig. 5. Note that in these experiments, the CAT was able to utilize the information from both the radar and connectivity.

A section on the Interstate 75 highway was selected for highway experiments as shown in Fig. 10(a). We had previously collected elevation data on this road using four GPS sensors attached to four vehicles. The averaged elevation profile is shown in Fig. 10(b) with two significant hills enabling the optimal-in-energy controller framework to leverage gravitational potential energy.

In highway experiments we employed a PCC box as a part of our nominal controller. The PCC box hardware hosts the commercialized version of the PCC algorithm described in Section III-C and it is available for trucks manufactured by Navistar [45]. While details about the algorithm running under the PCC box are omitted here due to its confidential nature, it utilizes the road slope information to calculate the optimal-in-energy speed profile similar to the optimal control framework (24), but

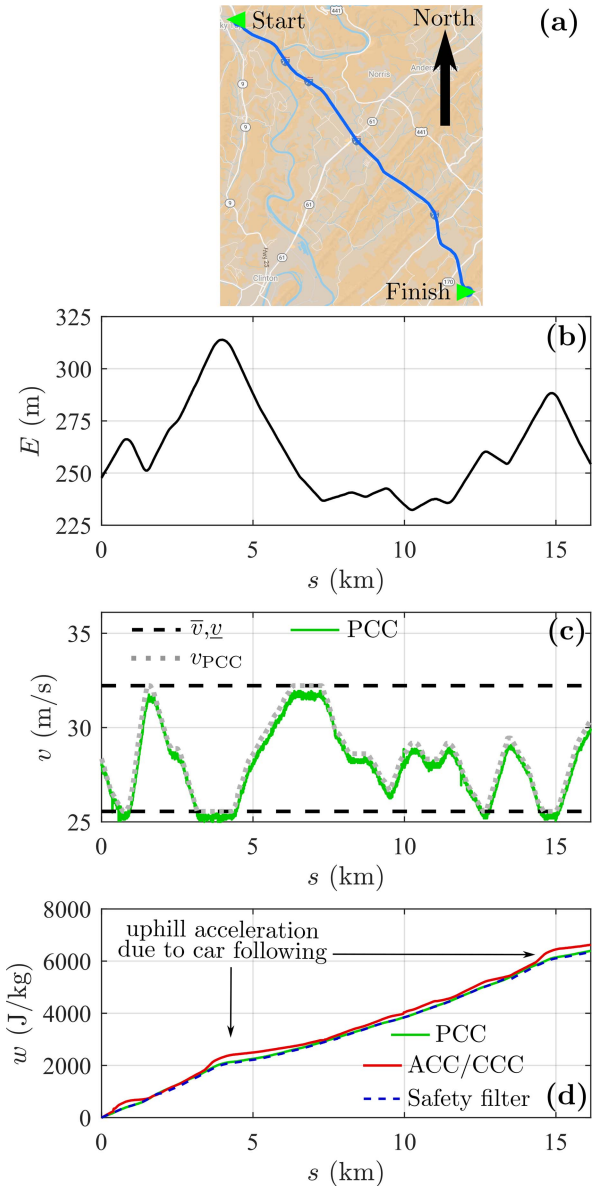


Fig. 10. (a) Section of I-75 used for the highway experiments. (b) Elevation profile E . (c) Speed limits \underline{v} and \bar{v} within which the PCC box operates, optimal-in-energy speed profile v_{PCC} , and measured CAT speed profile v in the PCC experiments. (d) Energy consumption curves w calculated from experimental data using (23) for different controllers.

TABLE IV
CONTROLLER PARAMETERS USED FOR THE HIGHWAY EXPERIMENTS

h_{st}	5 m	α_{CC}	0.7 1/s	\underline{v}	25 m/s
κ	0.8 1/s	α	0.2 1/s	\bar{v}	32 m/s
δ	20 m	β	0.5 1/s	\bar{u}	2 m/s ²
				\underline{u}	3 m/s ²

in a rolling horizon fashion. We used the desired speed values calculated by the PCC box as v_{PCC} in our variable-speed cruise controller structure (25). The PCC box enabled us to choose the speed limits \bar{v} and \underline{v} for our system; please refer to Table IV for these and all the other parameters used in highway experiments.

TABLE V
SUMMARY OF HIGHWAY EXPERIMENTAL RESULTS

Controller	Final energy consumption value	Energy saving compared to ACC/CCC	Finish time
PCC	6396 J/kg	3.6 %	579 s
ACC/CCC	6635 J/kg	-	577 s
Safety filter	6350 J/kg	4.3 %	583 s

The resulting optimal-in-energy speed profile is shown in Fig. 10(c) as a gray dotted curve. Similar to the on-track experiments, one may notice the variation of the optimal speed responding to the elevation changes along the road while obeying the speed limits.

B. Results

First, we implemented the PCC (25) using the speed profile v_{PCC} attained from the PCC box. Results are depicted in Fig. 10(c) as a green curve. Observe the good speed-tracking performance with a small steady-state error (up to 0.5 m/s). This error arose due to aerodynamics, which was more prominent at higher speeds than the low-speed experiments conducted when constructing the feedforward maps in the low-level controller. The energy consumption profile corresponding to the PCC run is displayed in Fig. 10(d) as a green curve. Here, the favorable energy consumption can be observed even at uphill regions thanks to the optimal speed profile taking the elevation profile into account. Table V summarizes the final energy consumption values in the highway experiments.

We remark that the environmental effects that lead to more drastic speed changes (thus better chance for the PCC to gain energy) were amplified in the closed track experiments through lead vehicle's speed profile design, see Figs. 6 and 7. In the public road test, on the other hand, the limited environmental effects (no traffic lights, conflicts by highway merging avoided by changing lanes) yielded more smooth driving conditions. Therefore, the positive impact of the PCC stayed on the lower ends of the range of potential benefits in longer distances.

Next, we present the results of the highway experiment when employing only safety-oriented controllers: the radar-based ACC and connectivity-based CCC without the PCC (from here on referred to as ACC/CCC). Note that in this case we still apply the safety filter (27) to integrate ACC and CCC in a seamless fashion; see Fig. 2. Similar to the on-track experiments, we employed a single CV agent in the scenario of Fig. 1(b) with a speed profile that includes uphill acceleration actions at around 3 km and 14.5 km; see Fig. 11(b). Another criterion in designing the CV speed profile was to have a similar finish time as the PCC run to avoid penalizing time for energy efficiency.

The distance headways and the speeds for the ACC/CCC run are given in Fig. 11(a) and (b), respectively. Good car-following performance can be observed in keeping the desired distance headway specified by the inverse of the range policy (14), i.e., $V^{-1}(v)$, depicted as orange dotted curve in panel (a). The ACC/CCC controller maintains a close track of the

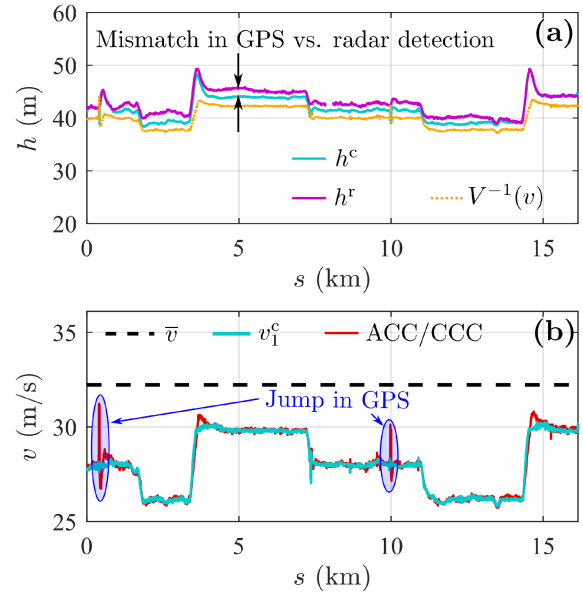


Fig. 11. Highway experimental results for the ACC/CCC experiments. (a) Connectivity-based distance headway h^c and radar-based distance headway h^r . (b) Speed limit \bar{v} , CV speed profile v_1^c and CAT speed profile v measured in the experiments.

velocity of the preceding vehicle v_1^c (cyan curve in panel (b)). In panel (a) the headway measured by the radar h^r (magenta) and calculated from connectivity h^c (cyan) show a small mismatch (up to 3.5 m). The safety filter (27) handles these inconsistencies by passing the controller that demands the most safety-critical acceleration. We note the jumps in the measured data in two separate time instances, highlighted in Fig. 11(b), were merely a malfunction in GPS sensing, and they did not influence the experiments significantly. Enforcing robustness against these types of impurities is a future research direction.

The energy consumption profile calculated for the ACC/CCC run given in Fig. 10(d) as a red curve, where the effect of the uphill acceleration due to following the energy-adverse CV speed profile is highlighted. The goal of finishing the course in a similar time as the PCC run was achieved as shown in Table V, and the truck's similar initial and final speeds for both experiments imply that an energy saving of 3.6% has been accomplished via using PCC over ACC/CCC.

Finally, we implemented the safety filter (27) with the PCC, ACC, and CCC. The CV followed the same speed profile as above (cyan curve in Fig. 11(b)). Results are presented in Fig. 12, where panel (a) shows the elevation profile of the road, while panel (b) depicts headway measured by the radar h^r (magenta) and calculated from connectivity h^c (cyan) as well as the target headway specified by the inverse of the range policy (orange dotted). When the cyan and magenta curves coincide, it indicates no vehicle between the truck and the CV; cf. the scenario depicted in Fig. 1(b). When engaged with a preceding vehicle, the safety filter successfully keeps the distance headway around the target value. While the radar sensing range restriction can be seen in this plot, the communication between V2X units continued over a distance of 300 m.

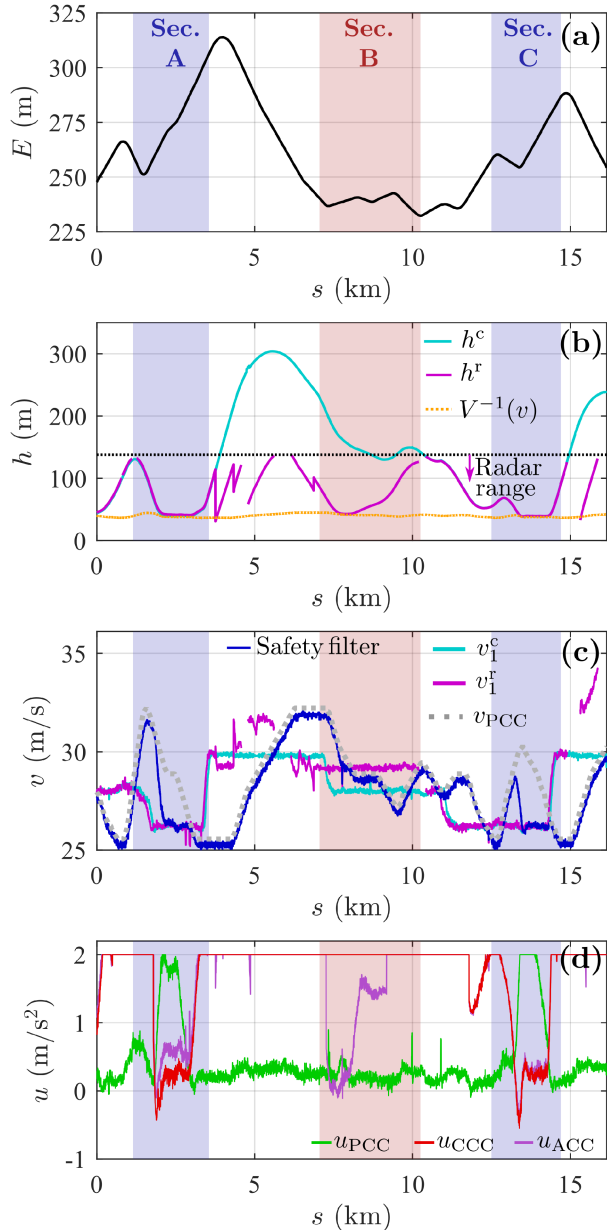


Fig. 12. Highway experimental results with the safety filter (27) employed. (a) Elevation profile E . (b) Connectivity-based distance headway h^c and radar-based distance headway h^r . (c) CV speed based on GPS v_1^c , preceding vehicle speed detected by radar v_1^r , optimal-in-energy speed profile v_{PCC} and measured speed v of the truck. (d) Controller outputs u_{PCC} , u_{CCC} and u_{ACC} . The safety filter passed the minimum of these.

Fig. 12(c) shows the speed signals of interest: the CV speed captured by connectivity v_1^c (cyan), the speed of the closest preceding vehicle detected by radar v_1^r (magenta), the optimal speed profile calculated by the PCC box v_{PCC} (gray dotted), and the measured speed v of the truck (blue). Panel (d) presents the controller outputs u_{PCC} (green), u_{CCC} (red), and u_{ACC} (magenta). Gaps in radar signals correspond to no vehicle detection in front, and sudden jumps indicate cut-ins from the other lanes. At some of these cut-ins, the lane-changing vehicle traveled faster than the truck (e.g., between 4–7 km and at 15.5 km),

which was not considered safety-critical by ACC, and therefore the safety filter kept using the PCC. As a matter of fact, one may notice in panel (d) that PCC was the active controller throughout the majority of the run, resulting in a comparable energy consumption to the PCC run, as shown by the blue dashed curve in Fig. 10(d). The energy saving compared to the CCC run is 4.3% without significantly increasing the course finish time, cf. Table V.

Switches to the safety-oriented controllers (i.e., to ACC or CCC) occurred at three separate locations: at 2 km, 7.5 km, and 13 km. While the first and the last engagements were between the CAT and the CV, in case of the middle one the truck responded to another non-connected vehicle traveling in the traffic. In the first occurrence, highlighted as Section I in Fig. 12, the PCC was initially the active controller. Then, the CV reduced its speed allowing the truck to catch up and engage. Consequently, the truck finished tracking the optimal speed profile and started following the CV with CCC (as the connectivity-based headway was reading a slightly smaller value than the radar-based headway, i.e., $h^c < h^r$). Then, the optimal speed profile gradually declined in the uphill section, favoring the PCC over CCC in the safety filter. Thus the CAT avoided uphill acceleration once the CV increased its speed. In the second switch sequence, labeled as Section II, the ACC briefly engaged with a non-connected vehicle traveling between the CV and truck, see the scenario depicted in Fig. 1(c). With time, the optimal speed became less than the preceding vehicle's speed, resulting in the PCC becoming the active controller again. The last switching sequence at 13 km, highlighted as Section III, occurred in a similar order as Section I. A video highlighting the events in Section I is available online [44].

VI. CONCLUSION

In this article, we proposed a safe integration scheme that integrates a performance-based nominal controller with safety-oriented controllers in a seamless manner for the longitudinal control of connected automated trucks (CATs). We established connections between the proposed integration scheme and the framework of control barrier functions that provides formal safety guarantees for controllers. The design steps of a performance-based predictive cruise controller (PCC) and a safety-oriented connected cruise controller (CCC) were detailed as exemplary controllers. We validated the proposed integration method in two experimental campaigns in low-speed and high-speed settings. In these experiments, we showed that the energy efficiency acquired through the PCC can be integrated with the safety provided by the CCC, with up to 18% and 4.3% savings in energy consumption for low-speed and high-speed driving cycles, respectively. Importantly, these experimental campaigns include a public highway, which highlights the potential of the proposed scheme to be implemented with commercial controllers of CATs in real-life driving scenarios.

Future work includes integrating more sophisticated performance-based controllers with a safety-critical controller. The robustness of these controllers against impurities such as GPS jumps will be investigated in detail.

APPENDIX A

CONTROL BARRIER FUNCTIONS AND SAFETY FILTER

Consider a nonlinear system of the form:

$$\dot{x} = f(x) + g(x)u, \quad (29)$$

with state $x \in \mathbb{R}^n$ and input $u \in \mathbb{R}^m$ along with a set $\mathcal{C} \subset \mathbb{R}^n$ defined as the 0-superlevel set of a continuously differentiable function $b : \mathbb{R}^n \rightarrow \mathbb{R}$:

$$\mathcal{C} \triangleq \{x \in \mathbb{R}^n \mid b(x) \geq 0\}. \quad (30)$$

System (29) is said to be *safe* with respect to the set \mathcal{C} if the following holds: $x(t_0) \in \mathcal{C} \Rightarrow x(t) \in \mathcal{C}$ for all $t \geq t_0$. We name the set \mathcal{C} as *safe set*.

Definition 1 (Control Barrier Function, [24]): The function b is a *Control Barrier Function (CBF)* for (29) on \mathcal{C} if there exists $\alpha \in \mathcal{K}$ such that for all $x \in \mathbb{R}^n$:

$$\sup_{u \in \mathbb{R}^m} \underbrace{\nabla b(x) \cdot (f(x) + g(x)u)}_{b(x,u)} > -\alpha(b(x)). \quad (31)$$

We note that a continuous function α is said to belong to class \mathcal{K} ($\alpha \in \mathcal{K}$) if $\alpha(0) = 0$ and α is strictly monotonically increasing. As stated by Corollary 2 in [24], a controller from the set of controllers given as:

$$K_{\text{CBF}}(x) \triangleq \left\{ u \in \mathbb{R}^m \mid \dot{b}(x, u) \geq -\alpha(b(x)) \right\} \quad (32)$$

renders the system (29) safe with respect to \mathcal{C} .

Consider the quadratic program (QP):

$$\begin{aligned} u^*(x) &= \underset{u \in \mathbb{R}^m}{\operatorname{argmin}} \frac{1}{2} \|u - u_{\text{nom}}(x)\|_2^2 \\ \text{s.t.} \quad &\dot{b}(x, u) \geq -\alpha(b(x)), \end{aligned} \quad (33)$$

which yields the notion of *safety filters*. Here the controller u_{nom} denotes a nominal controller that has been designed to ensure performance without considering safety. The safety filter outputs the nominal controller as long as it satisfies the CBF condition, i.e., $u^*(x) = u_{\text{nom}}(x)$ for all x such that $u_{\text{nom}}(x) \in K_{\text{CBF}}(x)$ holds. Otherwise the output deviates as minimally as possible from the nominal controller.

The solution of the QP can be obtained in a closed-form [31]. For a single input system, $u \in \mathbb{R}$, this solution reads:

$$u^*(x) = \begin{cases} \max\{u_{\text{nom}}(x), u_{\text{safe}}(x)\} & \text{if } \nabla b(x) \cdot g(x) > 0, \\ \min\{u_{\text{nom}}(x), u_{\text{safe}}(x)\} & \text{if } \nabla b(x) \cdot g(x) < 0, \\ u_{\text{nom}}(x) & \text{if } \nabla b(x) \cdot g(x) = 0, \end{cases} \quad (34)$$

where

$$u_{\text{safe}}(x) = -\frac{\nabla b(x) \cdot f(x) + \alpha(b(x))}{\nabla b(x) \cdot g(x)}. \quad (35)$$

Considering model (6) and a CBF in the form (11), that corresponds to (30) with $x = [h, v, v_1]^\top$ and $b(x) = h - \rho(v, v_1)$, and using Assumption 1, one may obtain

$$\nabla b(x) \cdot g(x) < 0. \quad (36)$$

That is, the safety filter (34) is applicable for the car-following scenario yielding (12).

REFERENCES

- [1] T. Litman, "Autonomous vehicle implementation predictions: Implications for transport planning," 2022. [Online]. Available: <https://www.vtpi.org/avip.pdf>
- [2] C.-Y. Chan, "Advancements, prospects, and impacts of automated driving systems," *Int. J. Transp. Sci. Technol.*, vol. 6, no. 3, pp. 208–216, 2017.
- [3] A. Brown, J. Gonder, and B. Repac, "An analysis of possible energy impacts of automated vehicles," in *Road Vehicle Automation*. Cham, Switzerland: Springer, 2014, pp. 137–153.
- [4] National Highway Traffic Safety Administration, "National motor vehicle crash causation survey," U.S. Department of Transportation, Washington, DC, USA, Tech. Rep. DOT HS 811 059, Jul. 2008.
- [5] M. M. Morando, Q. Tian, L. T. Truong, and H. L. Vu, "Studying the safety impact of autonomous vehicles using simulation-based surrogate safety measures," *J. Adv. Transp.*, vol. 2018, 2018, Art. no. 6135183.
- [6] J. B. Cicchino, "Effectiveness of forward collision warning and autonomous emergency braking systems in reducing front-to-rear crash rates," *Accident Anal. Prevention*, vol. 99, pp. 142–152, 2017.
- [7] S. Xu and H. Peng, "Design, analysis, and experiments of preview path tracking control for autonomous vehicles," *IEEE Trans. Intell. Transp. Syst.*, vol. 21, no. 1, pp. 48–58, Jan. 2020.
- [8] E. Yurtsever, J. Lambert, A. Carballo, and K. Takeda, "A survey of autonomous driving: Common practices and emerging technologies," *IEEE Access*, vol. 8, pp. 58443–58469, 2020.
- [9] A. Talebpour and H. S. Mahmassani, "Influence of connected and autonomous vehicles on traffic flow stability and throughput," *Transp. Res. Part C*, vol. 71, pp. 143–163, 2016.
- [10] A. Vahidi and A. Sciarretta, "Energy saving potentials of connected and automated vehicles," *Transp. Res. Part C*, vol. 95, pp. 822–843, 2018.
- [11] A. Alam, B. Besselink, V. Turri, J. Mårtensson, and K. H. Johansson, "Heavy-duty vehicle platooning for sustainable freight transportation: A cooperative method to enhance safety and efficiency," *IEEE Control Syst. Mag.*, vol. 35, no. 6, pp. 34–56, Dec. 2015.
- [12] J. I. Ge, S. S. Avedisov, C. R. He, W. B. Qin, M. Sadeghpour, and G. Orosz, "Experimental validation of connected automated vehicle design among human-driven vehicles," *Transp. Res. Part C*, vol. 91, pp. 335–352, 2018.
- [13] E. Pelletier et al., "In-vehicle validation of heavy-duty vehicle fuel savings via a hierarchical predictive online controller," SAE, Warrendale, PA, USA, Tech. Papers 2021-01-0432, 2021.
- [14] C. R. He, J. I. Ge, and G. Orosz, "Fuel efficient connected cruise control for heavy-duty trucks in real traffic," *IEEE Trans. Control Syst. Technol.*, vol. 28, no. 6, pp. 2474–2481, Nov. 2020.
- [15] S. E. Li et al., "Performance enhanced predictive control for adaptive cruise control system considering road elevation information," *IEEE Trans. Intell. Veh.*, vol. 2, no. 3, pp. 150–160, Sep. 2017.
- [16] V. Turri, Y. Kim, J. Guanetti, K. H. Johansson, and F. Borrelli, "A model predictive controller for non-cooperative eco-platooning," in *Proc. IEEE Amer. Control Conf.*, 2017, pp. 2309–2314.
- [17] B. HomChaudhuri, A. Vahidi, and P. Pisu, "Fast model predictive control-based fuel efficient control strategy for a group of connected vehicles in urban road conditions," *IEEE Trans. Control Syst. Technol.*, vol. 25, no. 2, pp. 760–767, Mar. 2017.
- [18] J. Liu, P. Jayakumar, J. L. Stein, and T. Eral, "A nonlinear model predictive control formulation for obstacle avoidance in high-speed autonomous ground vehicles in unstructured environments," *Veh. Syst. Dyn.*, vol. 56, no. 6, pp. 853–882, 2018.
- [19] S. Magdici and M. Althoff, "Adaptive cruise control with safety guarantees for autonomous vehicles," *IFAC-PapersOnLine*, vol. 50, no. 1, pp. 5774–5781, 2017.
- [20] B. Groelke, C. Earnhardt, J. Borek, and C. Vermillion, "A predictive command governor-based adaptive cruise controller with collision avoidance for non-connected vehicle following," *IEEE Trans. Intell. Transp. Syst.*, vol. 23, no. 8, pp. 12276–12286, Aug. 2022.
- [21] P. Nilsson et al., "Correct-by-construction adaptive cruise control: Two approaches," *IEEE Trans. Control Syst. Technol.*, vol. 24, no. 4, pp. 1294–1307, Jul. 2016.
- [22] S. Riedmaier, T. Ponn, D. Ludwig, B. Schick, and F. Diermeyer, "Survey on scenario-based safety assessment of automated vehicles," *IEEE Access*, vol. 8, pp. 87456–87477, 2020.
- [23] M. Amoozadeh, H. Deng, C.-N. Chuah, H. M. Zhang, and D. Ghosal, "Platoon management with cooperative adaptive cruise control enabled by VANET," *Veh. Commun.*, vol. 2, no. 2, pp. 110–123, 2015.
- [24] A. D. Ames, X. Xu, J. W. Grizzle, and P. Tabuada, "Control barrier function based quadratic programs for safety critical systems," *IEEE Trans. Autom. Control*, vol. 62, no. 8, pp. 3861–3876, Aug. 2017.

- [25] R. Isermann, R. Schwarz, and S. Stolz, "Fault-tolerant drive-by-wire systems," *IEEE Control Syst. Mag.*, vol. 22, no. 5, pp. 64–81, Oct. 2002.
- [26] International-Trucks, "Prostar truck," Accessed: Jun. 5, 2022. [Online]. Available: <https://www.internationaltrucks.com/trucks/prostar>
- [27] A. G. Ulsoy, H. Peng, and M. Çakmakci, *Automotive Control Systems*. Cambridge, U.K.: Cambridge Univ. Press, 2012.
- [28] Y. Li, D. Wu, J. Lee, M. Yang, and Y. Shi, "Analysis of the transition condition of rear-end collisions using time-to-collision index and vehicle trajectory data," *Accident Anal. Prevention*, vol. 144, 2020, Art. no. 105676.
- [29] T. J. Ayres, L. Li, D. Schleunig, and D. Young, "Preferred time-headway of highway drivers," in *Proc. IEEE 4th Int. Conf. Intell. Transp. Syst.*, 2001, pp. 826–829.
- [30] C. R. He and G. Orosz, "Safety guaranteed connected cruise control," in *Proc. IEEE 21st Int. Conf. Intell. Transp. Syst.*, 2018, pp. 549–554.
- [31] A. Alan, A. J. Taylor, C. R. He, A. D. Ames, and G. Orosz, "Control barrier functions and input-to-state safety with application to automated vehicles," *IEEE Trans. Control Syst. Technol.*, doi: [10.1109/TCST.2023.3286090](https://doi.org/10.1109/TCST.2023.3286090).
- [32] F. Blanchini and S. Miani, *Set-Theoretic Methods in Control*. Cham, Switzerland: Springer, 2008.
- [33] L. Zhang and G. Orosz, "Motif-based design for connected vehicle systems in presence of heterogeneous connectivity structures and time delays," *IEEE Trans. Intell. Transp. Syst.*, vol. 17, no. 6, pp. 1638–1651, Jun. 2016.
- [34] W. B. Qin, M. M. Gomez, and G. Orosz, "Stability and frequency response under stochastic communication delays with applications to connected cruise control design," *IEEE Trans. Intell. Transp. Syst.*, vol. 18, no. 2, pp. 388–403, Feb. 2017.
- [35] D. Hajdu, J. I. Ge, T. Insperger, and G. Orosz, "Robust design of connected cruise control among human-driven vehicles," *IEEE Trans. Intell. Transp. Syst.*, vol. 21, no. 2, pp. 749–761, Feb. 2020.
- [36] A. Sciarretta, G. De Nunzio, and L. L. Ojeda, "Optimal ecodriving control: Energy-efficient driving of road vehicles as an optimal control problem," *IEEE Control Syst. Mag.*, vol. 35, no. 5, pp. 71–90, Oct. 2015.
- [37] C. R. He, H. Maurer, and G. Orosz, "Fuel consumption optimization of heavy-duty vehicles with grade, wind, and traffic information," *J. Comput. Nonlinear Dyn.*, vol. 11, no. 6, 2016, Art. no. 061011.
- [38] A. Wächter and L. T. Biegler, "On the implementation of an interior-point filter line-search algorithm for large-scale nonlinear programming," *Math. Program.*, vol. 106, no. 1, pp. 25–57, 2006.
- [39] M. Shen, C. R. He, T. G. Molnar, A. H. Bell, and G. Orosz, "Energy-efficient connected cruise control with lean penetration of connected vehicles," *IEEE Trans. Intell. Transp. Syst.*, vol. 24, no. 4, pp. 4320–4332, Apr. 2023.
- [40] S. Wong, L. Jiang, R. Walters, T. G. Molnár, G. Orosz, and R. Yu, "Traffic forecasting using vehicle-to-vehicle communication," in *Proc. 3rd Conf. Learn. Dyn. Control*, 2021, pp. 917–929.
- [41] Truck Bus Control and Communications Network Committee, "Vehicle application layer," SAE International Paper J1939/71_202002, 2020, doi: [10.4271/J1939/71_202002](https://doi.org/10.4271/J1939/71_202002).
- [42] Speedgoat, "Mobile real-time target machine," Accessed: Jun. 5, 2022. [Online]. Available: <https://www.speedgoat.com/products-services/real-time-target-machines/mobile>
- [43] Commsignia, "V2X onboard unit," Accessed: Jun. 5, 2022. [Online]. Available: <https://www.commsignia.com/products/obu/>
- [44] "Video supplement for "experimental validation of safe multi-objective controller integration scheme for connected automated trucks," Accessed: Jun. 5, 2022. [Online]. Available: <https://youtu.be/Ae4hOsM0Mo4>
- [45] Navistar-Engine-Group, "International26 overview: Cruise control," 2017. [Online]. Available: https://www.internationaltrucks.com/-/media/Project/International-Trucks/International-Trucks/USA/General/Body-Builder/Engine-Media/EPA-17-International-A26/A26_CC.pdf



Anil Alan (Graduate Student Member, IEEE) received the B.Sc. degree in mechanical engineering from Middle East Technical University, Ankara, Turkey, in 2012, and the M.Sc. degree with Bilkent University, Ankara, in 2017. He is currently working toward the Ph.D. degree in mechanical engineering with the University of Michigan, Ann Arbor, MI, USA. His research interests include control of connected autonomous vehicles, robust safety-critical control, and vehicle dynamics.



Chaozhe R. He received the B.Sc. degree in applied mathematics from the Beijing University of Aeronautics and Astronautics, Beijing, China, in 2012, the M.Sc. and Ph.D. degrees in mechanical engineering from the University of Michigan, Ann Arbor, MI, USA, in 2015 and 2018, respectively. He is currently with Plus.ai Inc., Santa Clara, CA, USA, and working on planning and control algorithm development for automated trucking. His research interests include dynamics and control of connected automated vehicles, optimal and nonlinear control theory, and data-driven control.



Tamas G. Molnar (Member, IEEE) received the B.Sc. degree in mechatronics engineering, the M.Sc. and Ph.D. degrees in mechanical engineering from the Budapest University of Technology and Economics, Budapest, Hungary, in 2013, 2015 and 2018, respectively. Between 2018 and 2020, he held Postdoctoral position with the University of Michigan, Ann Arbor, MI, USA. Since 2020, he has been a Postdoctoral Fellow with the California Institute of Technology, Pasadena, CA, USA. His research interests include nonlinear dynamics and control, safety-critical control, and time delay systems with applications to connected automated vehicles, robotic systems, and machine tool vibrations.



Johaán Chacko Mathew received the B.Tech. degree in mechanical engineering from the Indian Institute of Technology Madras, Madras, India, in 2018, and the M.S. degree in mechanical engineering from the University of Michigan, Ann Arbor, MI, USA, in 2020. He is currently with Visteon Corporation as a Member of their motion controls and execution team in their advanced driver-assistance (ADAS) Program. His research interests include system modeling, identification, and control of dynamical systems, mechatronic systems, and vehicle dynamics.



A. Harvey Bell received the bachelor's degree from the University of Michigan, Ann Arbor, MI, USA. He pursued graduate studies with the University of Pennsylvania, Philadelphia, PA, USA. He is currently a Charles S and Ann S Hutchins Professor of Practice in Engineering with the University of Michigan, where he is also the Co-Director of the Multidisciplinary Design Program. He spent his 39-year long career in the automotive industry with General Motors where some of his significant achievements were: Chief Engineering a 2.5 Liter Engine, Vehicle Chief Engineering the 4th Generation Camaro and Firebird, Executive Director of the Advanced Vehicle Development Center for North America.



Gábor Orosz (Senior Member, IEEE) received the M.Sc. degree in engineering physics from the Budapest University of Technology, Budapest, Hungary, in 2002, and the Ph.D. degree in engineering mathematics from the University of Bristol, Bristol, U.K., in 2006. He held postdoctoral Positions with the University of Exeter, U.K., and the University of California, Santa Barbara, CA, USA. In 2010, he joined the University of Michigan, Ann Arbor, MI, USA, where he is currently an Associate Professor of mechanical engineering and civil and environmental engineering. From 2017 to 2018, he was a Visiting Professor of control and dynamical systems with the California Institute of Technology, Pasadena, CA, USA. In 2022, he was a Visiting Professor of applied mechanics with the Budapest University of Technology. His research interests include nonlinear dynamics and control, time delay systems, machine learning and data-driven systems with applications to connected and automated vehicles, traffic flow, and biological networks.